

# ZnO/SiO<sub>2</sub> microcavity modulator on silicon

P. D. Batista, B. Drescher, W. Seidel, J. Rudolph, S. Jiao, and P. V. Santos<sup>a)</sup>,

*Paul-Drude-Institut für Festkörperelektronik,  
Hausvogteiplatz 5–7, D-10117 Berlin, Germany*

(Dated: February 6, 2008)

## Abstract

We demonstrate a monolithic acousto-optic light modulator on silicon consisting of a piezoelectric ZnO/SiO<sub>2</sub> microcavity (MC) excited by a surface acoustic wave (SAW). The modulation of the MC optical resonance by the SAW creates an optical grating on the MC, which efficiently diffracts light beams impinging at the Bragg angle.

PACS numbers: 77.65.Dq 42.79.Jq 42.79.Hp 68.60.Bs

---

<sup>a)</sup>e-mail:santos@pdi-berlin.de

Resonant acousto-optics takes advantage of photonic<sup>1-3</sup> or electronic<sup>4,5</sup> resonances to enhance the coupling between optical and acoustic waves. A basic realization of this concept employs planar microcavity (MC) resonators of the type illustrated in Fig. 1(a), which consist of a  $\lambda/2$  cavity spacer (C) of thickness  $d_c$  and refractive index  $n_c$  inserted between two Bragg mirror (BM) stacks of dielectric and simultaneously, piezoelectric  $\lambda/4$  layers. A surface acoustic wave (SAW) generated on the structure by an interdigitated transducer (IDT) creates an optical superlattice (SL) by modulating the microcavity resonance wavelength  $\lambda_L = 2n_c d_c$  with a periodicity given by the acoustic wavelength  $\lambda_{\text{SAW}}$ . The MCs can be used for optical control by using the stop bands of the acoustically defined SL to back-diffract light impinging at the Bragg angle ( $\theta_B$ ), as indicated in Fig. 1(a).

Microcavity-based light modulators of the type in Fig. 1(a), fabricated using epitaxially-grown (Al,Ga)As structures, have intensity ratios  $R_1$  between impinging and back-diffracted light beams approaching 50%.<sup>3,6</sup> Their fabrication requires piezoelectric layers with a high refractive index contrast to allow for SAW generation as well as the formation of an efficient optical resonator. In this letter, we demonstrate the realization of monolithic MC modulators based on piezoelectric ZnO/SiO<sub>2</sub> layer stacks deposited via a low-temperature sputtering process. These MCs can be deposited on a wide range of substrates, including non-piezoelectric ones like Si. As in Fig. 1(a), the SAWs are generated by IDTs deposited on top of the piezoelectric MC. The diffraction efficiency  $R_1$  of the optical gratings induced by the SAW on ZnO/SiO<sub>2</sub> MCs on Si reaches a few percent. We show that the efficiency as well as its polarization dependence are well-explained by taking into account the modulation of the thickness and dielectric properties of the MC layers.

The ZnO and SiO<sub>2</sub> MC layers were deposited by rf-magnetron sputtering from ZnO and SiO<sub>2</sub> targets, respectively, on high-resistivity Si substrates at 200°C using an Ar/O<sub>2</sub> gas mixture. The deposition conditions for the ZnO layers were optimized in order to yield columnar-like crystallites with the hexagonal *c*-axis preferentially oriented along the growth direction. This preferential orientation is required for piezoelectricity and was verified by x-ray diffraction measurements. Figure 1(b) displays a cross-section scanning electron micrograph of a ZnO/SiO<sub>2</sub> MC designed for  $\lambda_L \sim 820$  nm. The BMs consist of 7 double stacks, each containing a 104 nm-thick ZnO and a 134 nm-thick SiO<sub>2</sub>  $\lambda/4$  layer and enclose a  $\lambda/2$  ZnO spacer.

SAWs with an acoustic wavelength  $\lambda_{\text{SAW}} = 5.6 \mu\text{m}$  and propagating along the  $x =$

[110] direction of the (001) Si substrate were generated by Al split-finger IDTs defined by photo-lithography on top of the ZnO/SiO<sub>2</sub> MCs. The rf-reflection coefficient  $s_{11}$  of the IDT [Fig. 2(a)] displays a series of resonance dips (denoted as  $M_1$  to  $M_3$ ) corresponding to the excitation of piezoelectric surface acoustic modes in the MC structures. In addition to the three modes in Fig. 2(a), a fourth mode was detected at 1.528 GHz and attributed to the excitation of a  $M_1$ -like mode with one third of the acoustic wavelength of the split-finger IDT.

The acoustic field distribution for each one of the modes was obtained from calculations of the elastic properties of the MC structure using the elastic continuum model described in Ref. 1. In the calculations, we assumed values for the elastic constants, densities, and piezoelectric coupling coefficient in the layers equal to those measured in the corresponding bulk materials.<sup>8</sup> The calculations yield piezoelectric SAW modes with calculated frequencies  $M_1^c = 544$  MHz,  $M_2^c = 842$  MHz, and  $M_3^c = 1010$  MHz, which are close to the measured modes  $M_1$  to  $M_3$ , respectively, in Fig. 2(a).<sup>9</sup> These modes are Rayleigh-like with acoustic displacements in the plane defined by the propagation ( $x$ ) direction and the surface normal ( $z$ -direction). The small differences between the calculated and measured mode frequencies are attributed to deviations in the elastic constants and density of the sputtered amorphous SiO<sub>2</sub> layers. The calculated depth distribution of the acoustic power density  $e_a$  for  $M_1^c$  to  $M_3^c$  is plotted in Fig. 2(b). These profiles were determined for a SAW with a linear power density  $P_\ell = 1000$  W/m (defined as the acoustic power per unit length along the cross section of the SAW beam of 120  $\mu\text{m}$ ). Due to the high acoustic velocity of the Si substrate, the MC acts as the core of an asymmetric waveguide (WG), which confines the acoustic modes between the surface and the substrate. Mode  $M_1^c$  is the fundamental WG mode with a single maximum within the MC structure.  $M_2^c$  and  $M_3^c$  are the second and third transverse modes with two and three maxima, respectively. Note that the penetration depth into the Si substrate increases with the transverse order.

The optical properties of the MCs as well as their operation as a light modulator were investigated by using a low-magnification ( $2\times$ , NA=0.055) microscope objective to create a wide (diameter of approx. 100  $\mu\text{m}$ ) and quasi-collimated white spot on the SAW path. The reflected light was collected by the same objective, spectrally and polarization analyzed, and detected by a multichannel spectrometer. The optical reflectivity  $R_0^y$  measured under normal incidence for light polarized along  $y$  is displayed by the solid line in Fig. 3(a). The

cavity reflection resonance dip at 800 nm has a quality factor  $Q = 300$  and is located within the 200 nm-wide stop band created by the BMs (the reflectivity data was normalized to unity within the stop band).

The excitation of the MC by the SAW leads to small changes in the optical reflectivity [dashed line in Fig. 3(a)], which can be better observed in the difference spectrum in the lower part of the figure. These spectra were obtained for light polarized along  $y$  (cf. inset) under excitation of mode  $M_2$  with  $P_\ell = 1420$  W/m. The reflectivity changes induced by this mode were found to be much stronger than for  $M_1$  and  $M_3$ .

In contrast to the small changes in the normal incidence reflectivity, much larger effects are observed in spectra recorded at the Bragg incidence angle  $\theta_B = \arctan[\lambda_L/(2\lambda_{\text{SAW}})]$ . Here, the incoming beam is Bragg-diffracted on the SAW grating, leading to a diffracted beam  $R_1$  propagating in the direction opposite to the incident one [cf. inset of Fig. 3(b)]. Figure 3(b) shows diffraction spectra for the  $y$  polarization ( $R_1^y$ ) recorded for different acoustic powers. The  $R_1^y$  peak only appears under SAW excitation. Its spectral position is blue-shifted relative to  $R_0^y$ , as expected for diffraction from modes at the border of the mini-Brillouin zone defined by the SAW.<sup>1,3</sup> In addition, its intensity increases linearly with acoustic power and is stronger for polarization along  $y$  than along  $x$ , as illustrated in Fig. 3(c)].

The diffraction intensity in Fig. 3 as well as its polarization dependence can be qualitatively understood by taking into account the acousto-optic interaction between the SAW and the optical field for photon energies close to the MC resonance wavelength. The light field  $E$  in the ZnO cavity layer is strongly enhanced by the MC. This effect is indicated in the lower curve in Fig. 4, which displays  $|E|^2$  (normalized to the intensity of the input beam) at the resonance wavelength  $\lambda_c = n_c d_c$  for normal incidence. During the propagation across a layer with thickness  $d_i \ll \lambda_{\text{SAW}}$  centered at a depth  $z_i$ , a light beam experiences a SAW-induced phase shift with amplitude given by  $\frac{\delta\Delta\phi^{(\rho)}}{\Delta\phi}(z_i) = \frac{\Delta n^{(\rho)}}{n}(z_i) + \varepsilon_{zz}(z_i)$ . The first term on the right-hand-side accounts for the elasto-optic modulation of the refractive index  $n$ , which depends on light polarization  $\rho(= x, y)$ . The second term describes the mechanical thickness changes associated with the SAW strain component  $\varepsilon_{zz}$  perpendicular to the layers. The phase modulation leads to relative changes in the resonance wavelength given by  $\frac{\Delta\lambda_0^{(\rho)}}{\lambda_0} \approx \frac{\delta\Delta\phi^{(\rho)}}{\Delta\phi}(z_c)$ , where  $z_c$  denotes the average cavity depth, as well as to a diffraction intensity  $R_1^{(\rho)} \propto \left[\frac{\delta\Delta\phi^{(\rho)}}{\Delta\phi}(z_c)\right]^2$ .

The calculated depth dependence of  $\frac{\delta\Delta\phi^{(\rho)}}{\Delta\phi}(z_i)$  for mode  $M_2^c$  is shown in Fig. 4. The

elasto-optic contribution is negligible for light field  $E$  along  $y$ ; the modulation in this case is essentially due the strain term  $\varepsilon_{zz}$ . The latter also dominates the modulation for the  $x$  polarization. The average values of  $\frac{\delta\Delta\phi^{(\rho)}}{\Delta\phi}(z_i)$  for  $\rho = x$  are lower than for  $\rho = y$  because of the small elasto-optic contribution, which has a sign opposite to the one associated with the strain. This polarization dependence is in agreement with the experimental results of Fig. 3(c). For a quantitative comparison with the experiments, we used the numerical approach described in Ref. 7 to determine the diffraction intensity from the values for the SAW strain and refractive index modulation displayed in Fig. 4.[8] The results, given by the lines in Fig. 3(c), reproduce reasonably well the measured values, particularly if one takes into account that no adjustable parameter has been used. The lower diffraction intensities as compared to (Al,Ga)As MCs<sup>5</sup> result from the lower Q-factor and can be compensated by increasing the number of stacks in the BMs.

In conclusion, we have demonstrated a monolithic acousto-optic modulator on Si based on the modulation of a ZnO/SiO<sub>2</sub> MC by a SAW. The modulation intensities can be well understood by taking into account the acousto-optic properties of the layers. High diffraction intensities are anticipated for higher acoustic intensities and Q-factors of the MCs.

We thank S. Fölsch for comments and for a critical reading of the manuscript as well as A.-K. Bluhm and U. Jahn for the microscopic images. Support from the DAAD-Germany and from EU Network of Excellence ePIXnet is gratefully acknowledged.

---

<sup>1</sup> M. M. de Lima, Jr. and P. V. Santos, Rep. Prog. Phys. **68**, 1639 (2005).

<sup>2</sup> M. Trigo, A. Bruchhausen, A. Fainstein, B. Jusserand, and V. Thierry-Mieg, Phys. Rev. Lett. **89**, 227402 (2002).

<sup>3</sup> M. M. de Lima, Jr., R. Hey, P. V. Santos, and A. Cantarero, Phys. Rev. Lett. **94**, 126805 (2005).

<sup>4</sup> A. L. Ivanov and P. B. Littlewood, Phys. Rev. Lett. **87**, 136403 (2001).

<sup>5</sup> M. M. de Lima, Jr., M. van der Poel, P. V. Santos, and J. M. Hvam, Phys. Rev. Lett. **97**, 045501 (2006).

<sup>6</sup> M. M. de Lima, Jr., R. Hey, and P. V. Santos, Appl. Phys. Lett. **83**, 2997 (2003).

<sup>7</sup> P. V. Santos, J. Appl. Phys. **89**, 5060 (2001).

<sup>8</sup> Details about the calculations will be given elsewhere

<sup>9</sup> In addition to the Rayleigh modes, the calculations predict the existence of two non-piezoelectric shear (i.e., Love-like) modes polarized along the  $y = [\bar{1}\bar{1}0]$  direction of the Si substrate, which cannot be excited by IDTs.

## Figure captions

Figure 1: (Color online) (a) Acoustically modulated microcavity (MC) consisting of a cavity layer (C) inserted in-between Bragg mirror (BM) stacks. The MC is modulated by a surface acoustic wave (SAW) launched by a piezoelectric transducer (IDT). The optical superlattice (SL) created by the SAW back-diffracts light beams impinging at the Bragg angle  $\theta_B$ . (b) Cross-section electron micrograph of a ZnO/SiO<sub>2</sub> MC grown on a (001) Si wafer.

Figure 2: (Color online) (a) Radio-frequency (rf) reflection coefficient  $s_{11}$  for IDTs on the MC of Fig. 1. (b) Calculated depth profiles for the acoustic power density  $e_a$  for the three Rayleigh modes ( $M_1^c$ - $M_3^c$ ) for a linear power density  $P_\ell = 1000$  W/m.

Figure 3: (Color online) (a) Normal reflectivity for  $y$  polarization ( $R_0^y$ ) in the absence (solid line) and presence of a SAW with  $P_\ell = 1420$  W/n. The lower curve displays the difference between the two spectra. (b) Back-diffraction spectra ( $R_1^y$ ) for different acoustic powers  $P_\ell$ , recorded at the Bragg angle (cf. inset). The curves are displaced vertically for clarity. (b) Back-diffraction peak intensity for polarization along  $x$  ( $R_1^x$ , squares, cf. inset) and  $y$  ( $R_1^y$ , dots) as a function of  $P_\ell$ . The lines are the corresponding calculated diffraction intensities.

Figure 4: (Color online) Depth dependence of  $\frac{\delta\Delta\phi^{(\rho)}}{\Delta\phi}(z) = \frac{\Delta n^{(\rho)}}{n}(z) + \varepsilon_{zz}(z)$  ( $\rho = x, y$ , left scale) and electric field amplitude  $|E|^2$  (right scale) calculated for mode  $M_2^c$  for  $P_\ell = 1000$  W/m.

## Figures

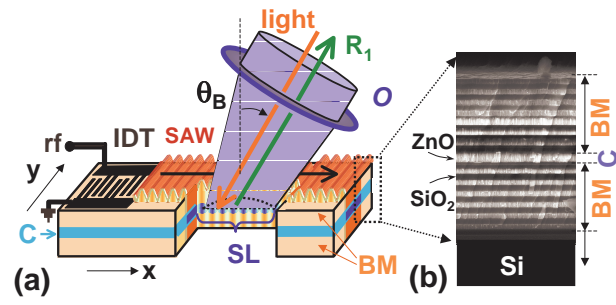


FIG. 1: Diniz *et al.*, ZnO/SiO<sub>2</sub> microcavity modulator on silicon



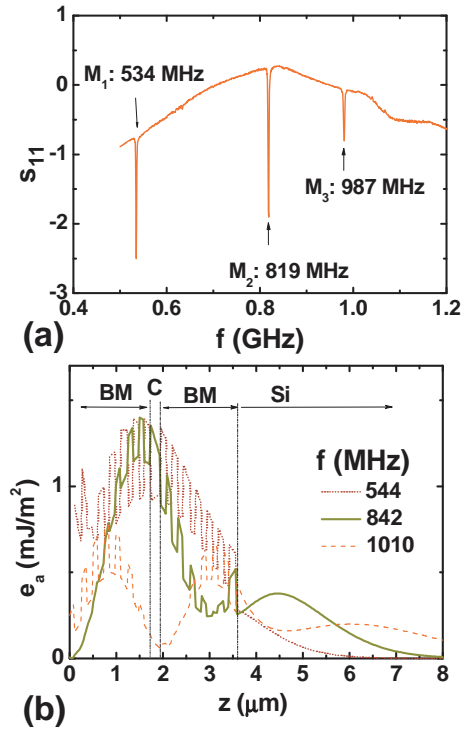


FIG. 2: Diniz *et al.*, ZnO/SiO<sub>2</sub> microcavity modulator on silicon

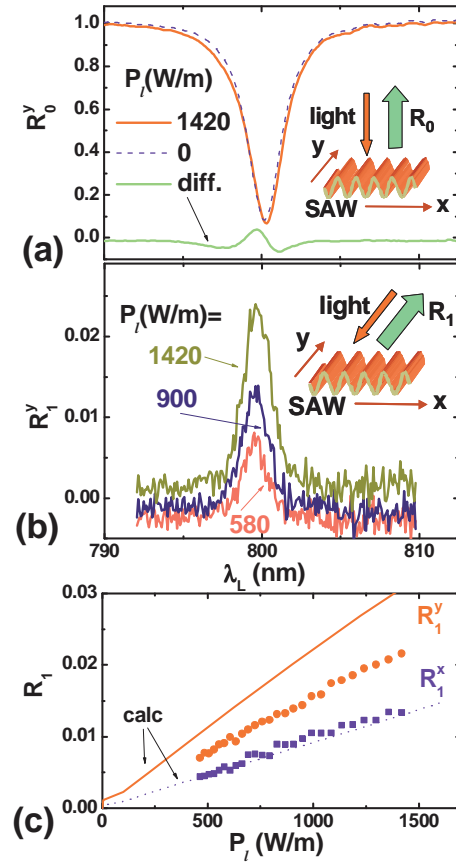


FIG. 3: Diniz *et al.*, ZnO/SiO<sub>2</sub> microcavity modulator on silicon

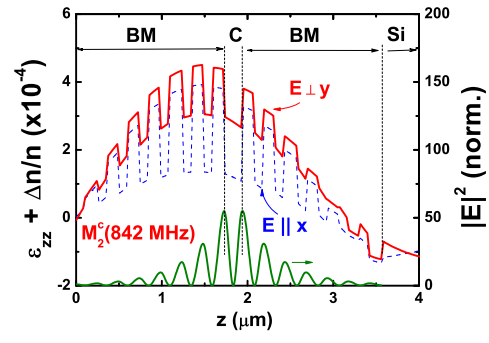


FIG. 4: Diniz *et al.*, ZnO/SiO<sub>2</sub> microcavity modulator on silicon